IEEE Photonics Journal
An IEEE Photonics Society Publication

Open Access

Interferograms of Votex FWM Beam for Nonlinear Spatial Filter in Photonic Band Gap

Volume 11, Number 1, February 2019

Zhiguo Wang
Yanyong Sun
Jiawei Yang
Yanpeng Zhang

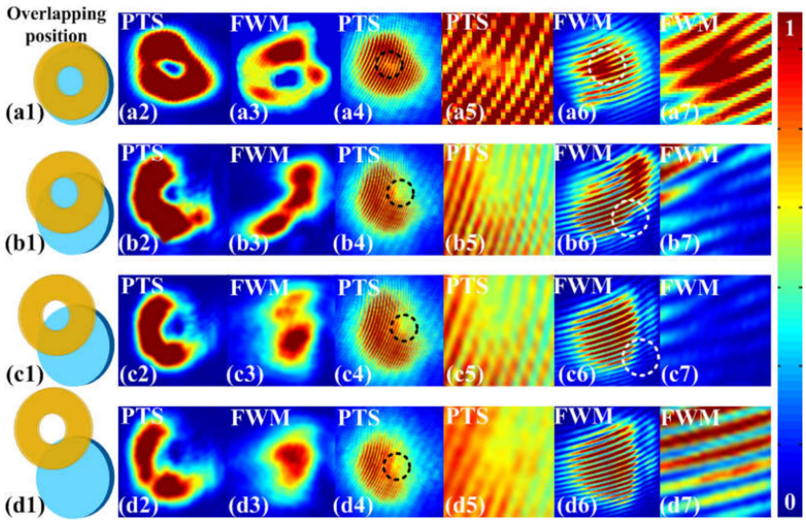

DOI: 10.1109/JPHOT.2018.2884453
1943-0655

IEEE photonics SOCIETY

IEEE

Interferograms of Votex FWM Beam for Nonlinear Spatial Filter in Photonic Band Gap

Zhiguo Wang,[1,2] **Yanyong Sun**,[1,2] **Jiawei Yang**,[1,2] **and Yanpeng Zhang** [1,2]

[1]Key Laboratory for Physical Electronics and Devices of the Ministry of Education and Shaanxi Key Lab of Information Photonic Technique, Xi'an Jiaotong University, Xi'an, Shaanxi 710049, China
[2]School of Electronic and Information Engineering, Xi'an Jiaotong University, Xi'an, Shaanxi 710049, China

DOI:10.1109/JPHOT.2018.2884453

Manuscript received August 23, 2018; revised October 18, 2018; accepted November 27, 2018. Date of publication December 3, 2018; date of current version December 28, 2018. This work was supported in part by the National Key R&D Program of China under Grant 2017YFA0303700, in part by the National Nature Science Foundation of China under Grants 61308015 and 11474228, in part by the Key Science and Technological Innovation Team of Shaanxi Province under Grant 2014KCT-10, and in part by the Fundamental Research Funds for the Central Universities under Grant xjj2016030. Corresponding authors: Zhiguo Wang and Yanpeng Zhang (e-mail: wangzg@mail.xjtu.edu.cn; ypzhang@mail.xjtu.edu.cn).

Abstract: We analyze the properties and interferograms of vortex four-wave mixing (FWM) beams by varying the incident angle of the probe field. Based on the properties, we propose the model of a new type of nonlinear spatial filter without diffraction using a Bragg grating in the nonlinear FWM process. We show the evolutions of shapes and interferograms of probe transmission signal (PTS) and FWM by scanning the probe detuning, and demonstrate the Kerr nonlinearity can manipulate the shapes and spatial location of vortex PTS and FWM images. Further, we can determine the center position of the new type of nonlinear filter through interference patterns and use the Kerr nonlinearity of related fields to control the nonlinear filter precisely. In addition, the interferograms of the reflected signal from the photonic band gap (PBG) structure are studied both in experiment and theory. We demonstrate that the number of fork-like patterns of reflected signal changes from one to three, revealing that the superposition of first-order and third-order beams in the reflected signal from PBG structure creates an inverted fork-like pattern.

Index Terms: Nonlinear optics, four-wave mixing, interference, coherent optical effects.

1. Introduction

In the past decade, there has been a great many of researches about the orbital angular momentum (OAM) [1], [2] since the first theory by Allen *et al.* which demonstrated that the Laguerre-Gaussian (LG) beam has a well-defined OAM [3]. The photons with OAM can possess prominent advantages such as compatibility with diverse quantum networks [4], Bose-Einstein condensates [5] and quantum optical communications [6]. The main properties of beams containing vortex phase singularities were analyzed by Soskin *et al.* and demonstrate the topological charge changing principle [7], [8]. In addition, for the optical vortex (OV), related researches involve electromagnetically induced transparency (EIT) [9], second-harmonic generation [10], stimulated down-conversion processes [11],

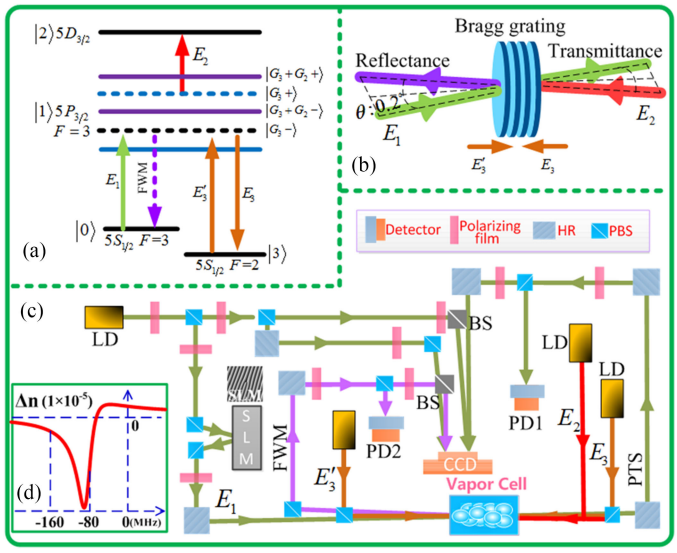

Fig. 1. (a) The cascade four-level atomic system and the light fields. (b) Periodic static standing wave pattern. (c) Precise experiment setup of our experiment. (d) The nonlinear refractive index induced by dressing field E_2.

[12] and four-wave mixing (FWM) processes [13], [14]. Moreover, the nonlinear Kerr effect on nonlinear beams has been investigated [15] in multilevel atomic systems, which can impose effects on the spatial intensity distribution of OV such as entangled states [16] and logical gates for quantum computation [17]. Besides, the study of OAM can be applied to micromanipulation techniques [18] and glimmer manipulation [19].

In this paper, we experimentally observe the vortex probe transmission signal (PTS) and FWM signals generated in a photonic band gap (PBG) structure. We propose a model of a new type of nonlinear spatial filter based on a Bragg grating in the nonlinear FWM process. By analysis of the spatial images and interference patterns of the vortex PTS and FWM signal with scanning the probe detuning, we not only explain the characteristics of the signal images such as defocusing, shift and splitting modulated by the Kerr nonlinearity, but also use the Kerr nonlinearity to control the new type of nonlinear filter. Besides, we demonstrate the fork-like pattern number of the reflected signal from the PBG structure can be modulated from one to three by the Kerr nonlinearity of dressing field.

2. Theoretical Model and Experimental Scheme

The experiment is conducted in a hot rubidium composed of 70% ^{85}Rb and 30% ^{87}Rb and based on a four-level inverted-Y atomic energy level system that includes $5S_{1/2}(F=3)(|0\rangle)$, $5P_{3/2}(F=3)(|1\rangle)$, $5D_{3/2}(|2\rangle)$ and $5S_{1/2}(F=2)(|3\rangle)$ as shown in Fig. 1(a). The probe laser field E_1 (wavelength $\lambda_1 = 780.243$ nm, frequency ω_1, wave vector $\mathbf{k}_1$, Rabi frequency G_1) connecting $|0\rangle$ and $|1\rangle$ is a Laguerre-Gaussian beam with the fixed topological charge m $= 1$. It carries OAMs of $+\mathrm{m}\hbar$ per photon after being modulated by SLM with fork-like phase patterns (the computer-generated phase hologram) [20] as depicted in Fig. 1(c). The amplitude of the Laguerre-Gaussian beam is given by

$$E_{LG} = A_1\left[\sqrt{2}r/\varpi\right]^{|m|} e^{-r^2/\varpi^2} \exp(im\theta) L_p^m\left[2r^2/\varpi^2\right], \tag{1}$$

where A_1 is the amplitude, ϖ is half beam width, r and θ are radial and azimuthal coordinates, L_p^m is Laguerre polynomial, p and m are the radial and azimuthal numbers with $p = 0$ in our experiment. The other two counter propagating coupling beams $E_3(\lambda_3 = 780.238$ nm, ω_3, $\mathbf{k}_3$, $G_3)$ and $E_3'(\lambda_3' = 780.238$ nm, ω_3, $\mathbf{k}'_3$, $G_3')$, which are from the same one laser, drives the transition

from $|1\rangle$ to $|3\rangle$. The weak probe beam E_1 propagates in the same direction of E_3' with a small angle θ (about 0.2°) going through the Rb vapor cell while E_3 propagates in the opposite direction of E_3' as shown in Fig. 1(b). As a result, a Bragg grating is generated in the medium leading to a PBG structure as shown in Fig. 1(b). Under this condition, we have a good observation of the transmitted signal (PTS signal) and the reflected signal which includes third-order signal (FWM) (phase-matching condition $\mathbf{k}_F = \mathbf{k}_1 + \mathbf{k}_3 - \mathbf{k}'_3$) and first-order signal [21]. Since the probe field's absorption background doesn't exist in the spectrum of the reflected signal and the intensity of the reflected signal is sensitive to the power of field E_3 and E_3' [22], we confirm that the third-order signal is the dominant in the reflected signal. The dressing laser beam E_2 ($\lambda_2 = 775.978$ nm, ω_2, $\mathbf{k}_2$, G_2) links an upper transition $|1\rangle$ and $|2\rangle$ having a small angle with E_3. Besides, according to the energy levels and the perturbation chain (Liouville pathway) theory, the first-order susceptibility related to the PTS and third-order nonlinear one related to the reflected FWM can be deducted from density matrix elements based on the relation $\varepsilon_o \chi E = N\mu\rho$ and $G = \mu E/\hbar$ in which E represents electric field; ε_0 and N are dielectric constant and the atom density; G and μ are the Rabi frequency and transition dipole moment, respectively. So the first-order and third-order susceptibilities can be obtained as [22]

$$\chi^{(1)} = \frac{iN\mu^2}{\hbar\varepsilon_0} \frac{1}{d_1 + |G_{3s}|^2/d_3 + |G_2|^2/d_2}, \tag{2}$$

$$\chi^{(3)} = -\frac{iN\mu^4}{\hbar\varepsilon_0} \frac{1}{(d_1 + |G_{3s}|^2/d_3 + |G_2|^2/d_2)^2 d_3}, \tag{3}$$

where $|G_{3s}|^2 = |G_3|^2 + |G_3'|^2 + 2G_3G_3'\cos(2k_3z)$, $d_1 = \Gamma_{10} + i\Delta_1$, $d_3 = \Gamma_{30} + i(\Delta_1 - \Delta_3)$, $d_2 = \Gamma_{20} + i(\Delta_1 + \Delta_2)$. Frequency detuning $\Delta_i = \Omega_i - \omega_i$ (Ω_i is the resonance frequency of the transition driven by beam E_i); Γ_{ij} is transverse relaxation rate between $|i\rangle$ and $|j\rangle$.

The beams of PTS and FWM can be modulated by nonlinear Kerr effect of related fields. Kerr nonlinear coefficient is expressed as $n_2 = \mathrm{Re}\chi^{(3)}/(\varepsilon_0 c n_1)$, with n_1 being the refractive index at ω_1; ε_0 being the dielectric constant. The nonlinear phase of PTS and FWM induced by strong field E_i is:

$$\varphi_{NL}(z, x, y) = 2\mathbf{k}_{1,F} n_2^{XE_i} I_i e^{-\xi^2} z/(n_1 I_{1,F,S}), \tag{4}$$

where z is the longitudinal coordinate in the propagation direction; $E_i (i = 3, 3', 2)$ represent relative strong fields; $n_2^{XE_i}$ ($n_2^{SE_i}$) are the cross-Kerr (self-Kerr) coefficients induced by E_i; $\xi = (x^2 + y^2)^{1/2}$ indicates the transverse dimension, and ω_0 is the spot size of relevant beam. Here, $\Delta n = n_2^{XE_i} I_i$ shows the nonlinear refractive index induced by E_i, e.g., the nonlinear refractive index induced by dressing field E_2 is shown as Fig. 1(d), where the value of the nonlinear refractive index is less than 0 around $\Delta_2 = -80$ MHz, and the absolute value get the maximum at the resonance point $\Delta_1 = -\Delta_2 = 80$ MHz. Furthermore, output PTS and FWM are related to nonlinear phase:

$$E_P \propto \chi^{(1)} e^{j\varphi_{NL}} E_1, \tag{5}$$

$$E_F \propto \chi^{(3)} e^{j\varphi_{NL}} E_1 E_3 E_3', \tag{6}$$

where E_1 consists of the spiral phase term. Besides, the topological charge conservation law must be considered. To write it,

$$m_F = m_1 + m_3 - m_3', \tag{7}$$

where $m_3 = m_3' = 0$ in the experiment.

3. Experimental Results and Theoretical Analyses

Figure 2 shows the process of tuning the FWM signal by varying the overlap of the probe field E_1 and Bragg grating which is implemented by changing the incident angle of the probe field E_1. The FWM is generated by the nonlinear process of E_1, E_3 and E_3' in which the probe field E_1 is

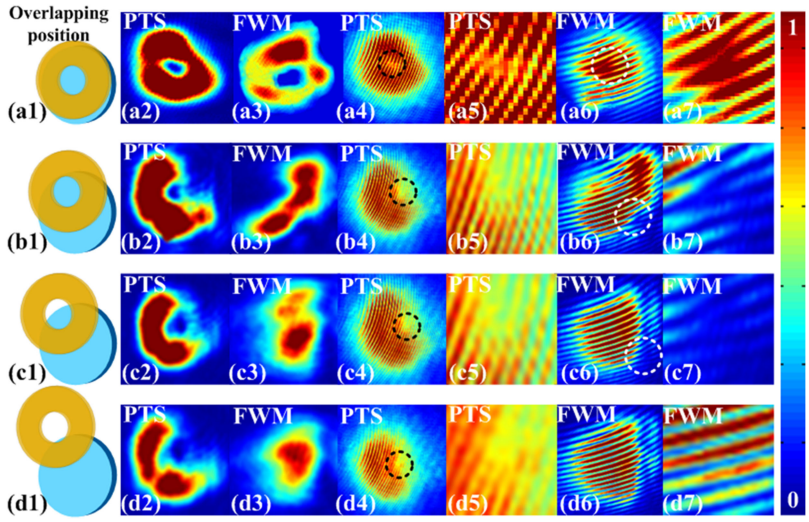

Fig. 2. (a1)–(d1) The overlapping position of vortex E_1 beam and Bragg grating (the yellow ring represents the vortex E_1 beam and the blue circle represents the left view of the Bragg grating). (a2)–(d2) The vortex PTS corresponds to (a1)–(d1), respectively. (a3)–(d3) The FWM corresponds to (a1)–(d1), respectively. (a4)–(d4) The interference patterns of PTS corresponds to (a2)–(d2), respectively. (a5)–(d5) The partial enlargement of fork-like patterns corresponds to (a4)–(d4), respectively. (a6)–(d6) The interference patterns of FWM corresponds to (a3)–(d3), respectively. (a7)–(d7) The partial enlargement of fork-like patterns corresponds to (a6)–(d6), respectively.

an OV signal. Therefore, the FWM is also an OV signal with the same frequency ω_1 with incident probe field according to the conservation law of the topological charge in Eq. (7) and its singularity location changes with the incident angle of probe field E_1, which can be detected by the fork-like patterns in the interferogram with a same-frequency reference Gaussian beam.

In Fig. 2(a1), the vortex probe field E_1 beam and the Bragg grating are completely overlapped. In this case, we can clearly see the shapes of the PTS and FWM are similar to donuts as shown in Fig. 2(a2) and 2(a3), respectively. At the same time, we can observe the fork-like patterns in PTS and FWM interferograms as shown in Fig. 2(a4) and 2(a6) (Fig. 2(a5) and 2(a7) are the partial enlargement of the fork-like patterns, respectively). Through comparing the fork-like pattern of FWM (Fig. 2(a6) and 2(a7)) with the PTS's (Fig. 2(a4) and 2(a6).), we demonstrate transfer of OAM from the probe field E_1 to FWM through the nonlinear FWM process.

Then, we change the overlap of the vortex probe field E_1 beam and the Bragg grating by adjusting the incident angle of the probe. In detail, we adjust the center (singularity) of probe field E_1 to overlap with the edge of the Bragg grating as shown in Fig. 2(b1). In this case, it's clear to see the shape of FWM in Fig. 2(b3) is destroyed into a semicircle compared with FWM in Fig. 2(a3), while the shape of vortex PTS is basically unchanged as shown in Fig. 2(a2) and 2(b2). Besides, by observing the interference patterns in Fig. 2(b6–b7), we can find the generated fork-like interference pattern is away from the center of the FWM as shown by the dotted circle in Fig. 2(b6). The destroyed shape and shifted fork-like pattern of FWM show that only the overlapped part of probe field E_1 with the Bragg grating participates in the FWM process. As the position of the vortex E_1 continues to move away from the Bragg grating as shown in Fig. 2(c1), the PTS beam remains basically unchanged as shown in Fig. 2(c2) while the FWM shape is seriously damaged in Fig. 2(c3). Simultaneously, the fork-like pattern of FWM in the lower right corner of the interference pattern is very weak as shown by the white dash line in Fig. 2(c6) (partial enlargement in Fig. 2(c7)). When the E_1 singularity moves outside the Bragg grating in Fig. 2(d1), the formed FWM is similar to an ordinary Gaussian beam in Fig. 2(d3) and it doesn't show the singularity according to the interference pattern as shown in Fig. 2(d7). From Figure 2, we can observe that the FWM fork-like interference pattern has changed from perfect to imperfect, due to the choice of the Bragg grating to OV signal.

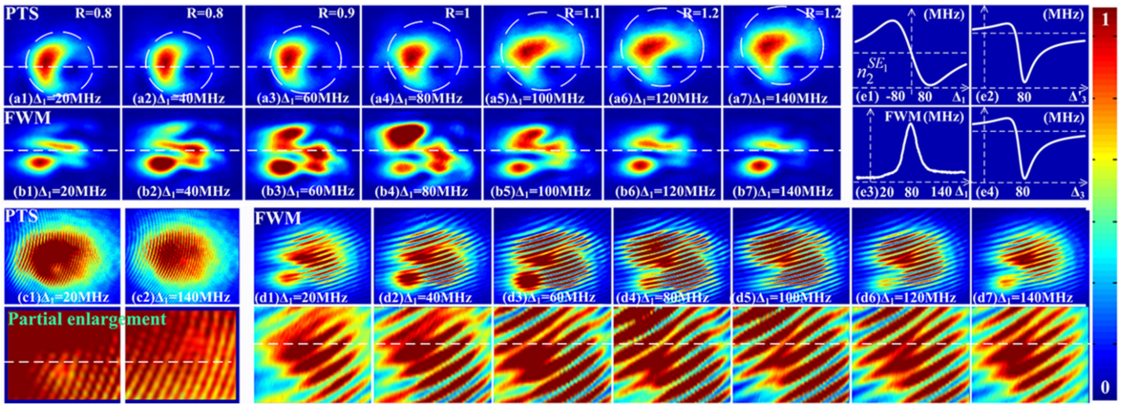

Fig. 3. (a1)–(a7) Evolutions of the vortex PTS by increasing Δ_1 from 20 to 140 MHz at $\Delta_3 = 80$ MHz. (b1)–(b7) Evolutions of the generated vortex FWM corresponding to (a1)–(a7), respectively. (c1)–(c2) The interference patterns of vortex PTS under $\Delta_1 = 20$ MHz and $\Delta_1 = 140$ MHz, respectively. (d1)–(d7) The interference patterns of vortex FWM correspond to (b1)–(b7). (e1) The self-Kerr coefficient of PTS beam. (e2), (e4) The nonlinear refractive index induced by field E_3' and E_3, respectively. (e3) Spectrum of the generated FWM versus the detuning Δ_1 at $\Delta_3 = 80$ MHz.

From Fig. 2, we propose a method to create a new type of nonlinear spatial filter based on the PBG structure in the nonlinear FWM process. We use the overlapping area of probe field E_1 and the Bragg grating as the filter. Furthermore, the incident probe E_1 beam is the input signal and the reflected signal beam passing through the filter is the output signal. We have defined that the size of the nonlinear filter is the diameter of overlapping area. In addition, the unchanged shapes of the output and input signals in Fig. 2(a2) and 2(a3) illustrate that the new type of nonlinear filter can eliminate diffraction compared with the traditional linear filter, such as aperture diaphragm. Next, we will use the nonlinear Kerr effect to precisely regulate this new type of nonlinear spatial filter.

In Fig. 3, we studied the detailed evolution of vortex PTS and FWM beams as well as their interferograms by scanning probe detuning Δ_1 around the resonance position $\Delta_1 = \Delta_3 = 80$ MHz. For the vortex PTS beam, as the detuning Δ_1 increases, we can see the area of the spot becomes larger and larger by observing the size of the blue background as shown by the white dash ovals (the diameter R of white dash oval is from 0.8 to 1.2) in Fig. 3(a1–a7). Actually, the spots locate in the defocus area with $\Delta_1 > 0$ MHz according to the nonlinear self-Kerr coefficient $n_2^{SE_1} < 0$ as shown in Fig. 3(e1). Moreover, with the increase of Δ_1, $|\Delta n_2^{SE_1}| = |n_2^{SE_1} I_1|$ gets larger and larger around $\Delta_1 = 80$ MHz, which is why the defocus phenomenon becomes more and more obvious as shown in Fig. 3(a). In addition, we also noticed that the PTS spot has a weak displacement along the y-direction with the detuning Δ_1 in Fig. 3(a). It is due to the cross-Kerr effect of the field E_3', which can control the PTS beam effectively in the EIT window generated by the probe and E_3' in the inverted-Y system according to $|G_{3s}|^2/d_3$ of $\chi^{(1)}$ in Eq. (2) as shown in Fig. 1(a). Specifically, the nonlinear phase of the vortex PTS signal is $\varphi_p = 2\mathbf{k}_1 n_2^{XE'_3} I'_3 e^{-\xi^2} z/(n_1 I_1)$, in which $|n_2^{XE'_3} I'_3|$ gets the maximum value at $\Delta_1 = \Delta_3 = 80$ MHz according to Fig. 3(e2). The additional the transverse wave vector $\delta_k = \partial\varphi_{3F}/\partial y < 0$ decides the repulsion of dressing field E_3' to PTS beam along y-direction and defocusing of PTS leads to a smaller I_1 in φ_p. Henceforth, the repulsion of E_3' is strong enough to cause the shifting of vortex PTS.

Then, we pay attention to the FWM spots in Fig. 3(b). We can observe the intensity of the FWM versus Δ_1 with $\Delta_3 = 80$ MHz is in accordance with the spectrum curve as shown in Fig. 3(e3). Moreover, it is obvious that the vortex FWM has a shifting along the y-direction when $\Delta_1 = 80$ MHz. Similar to the evolution of the PTS signal, the FWM is repulsed by the field E_3 in the EIT window produced by the FWM and E_3 in the inverted-Y system. By observing the FWM in Fig. 3(b), the largest shift occurs at $\Delta_1 = 80$ MHz because $|n_2^{XE_3} I_3|$ in the nonlinear phase of FWM $\varphi_{3F} = 2\mathbf{k}_F n_2^{XE_3} I_3 e^{-\xi^2} z/(n_1 I_F)$ reaches maximum according to the nonlinear refractive index of E_3 as shown

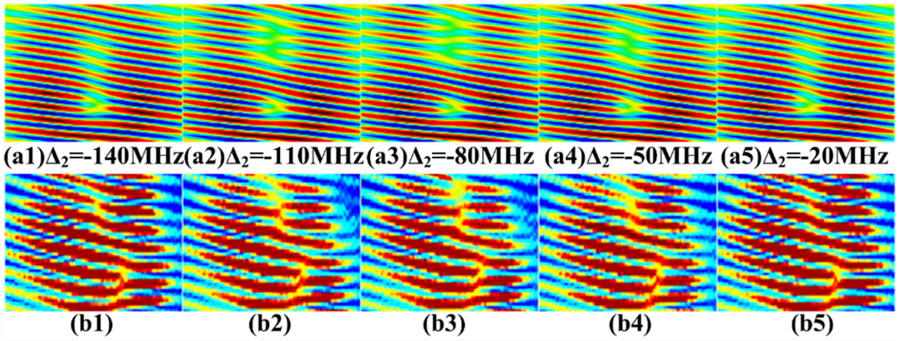

Fig. 4. (a1)–(a5) Simulation interference patterns of vortex reflected signal by increasing the detuning Δ_2 from -140 to -20 MHz at$\Delta_1 = \Delta_3 = 80$ MHz. (b1)–(b5) Experimental evolutions of the interference patterns of reflected signal corresponding to (a1)–(a5), respectively.

in Fig. 3(e4). Other than the shifting, we can observe that the shape of the FWM spot gradually changes from a two-petal spot to a three-petal spot at the resonance point $\Delta_1 = 80$ MHz. The nonlinear phase of FWM induced by E_3 caused not only the displacement, but also the splitting of the spot.

It is an effective way to observe the shifting of PTS and FWM signals through their interference with a same frequency Gaussian beam. Figures 3(c) and 3(d) are the interference patterns of vortex PTS beam and FWM beam versus detuning Δ_1, respectively. We can use the location of the singularity of PTS and FWM to visually observe the effect of the nonlinear phase. From PTS interference patterns as shown in Fig. 3(c), we can intuitively observe that the position and shape of the fork are basically unchanged. It is because the nonlinear effects on PTS are weak since probe is in the same order of magnitude strength as strong fields. But when we look closely at the partial enlargement in Fig. 3(c1) and 3(c2), which are corresponding to Fig. 3(a1) and 3(a7), we can see that there is a slight movement of the PTS singularity along the y-direction at $\Delta_1 = 20$ MHz and $\Delta_1 = 140$ MHz.The shifting of the fork-like patterns in Fig. 3(c) verifies the weak displacement of the PTS we described in Fig. 3(a). In contrast, FWM signal is much weaker compared with the PTS. So we can observe that the displacement of FWM singularity is more obvious in the interference patterns (the displacement reach the maximum at the resonance point $\Delta_1 = \Delta_3 = 80$ MHz as shown in Fig. 3(d4)).

From Fig. 3, we can resort to the Kerr nonlinearity of strong field (e.g, E_3') to make the probe shift precisely so as to control the size of the nonlinear filter. For example, we can accurately determine the incident signal spot in Fig. 3(a) moved up 0.5 mm with the strong field E_3' through measuring the interference patterns in Fig. 3(c). Thus we can get the selected output signal. More importantly, the diffraction during propagation can be eliminated by the self-Kerr nonlinearity after passing through the nonlinear filter through placing the input signal in the focus area, such as the one with $\Delta_1 < 0$ in Fig. 3(e1) [23].

In addition, the interferograms of the reflected signal from the PBG structure are studied both in theory and experiment as shown in Fig. 4. First, we adjust the incidence angle θ of E_1 from 0.2° to 0.15° in Fig. 4 compared with Fig. 3. Then, we theoretically analyze the interferograms of reflected signal containing first-order and third-order signals from the PBG structure by scanning the detuning Δ_2 as shown in Fig. 4(a). Topological charge is $+1$ for the leftward fork-like pattern in Fig. 4 and -1 for the rightward fork-like pattern. We can observe that the number of fork-like patterns of reflected signal changes with Δ_2 in theory. There is only one fork-like pattern of reflected signal, which indicates that the topological charge of reflected signal $m_R = +1$, in Fig. 4(a1) ($\Delta_2 = -140$ MHz) and 4(a5) ($\Delta_2 = -20$ MHz) when Δ_2 is far from the resonance point $\Delta_2 = -\Delta_1 = -80$ MHz. On the contrary, we can simulate the interference pattern of reflected signal with three fork-like patterns (including leftward, rightward, leftward fork-like patterns) along y-direction when the detuning Δ_2

meets the resonance point $\Delta_2 = -80$ MHz as shown in Fig. 4(a3). To explain the above phenomena, we need to mention the difference between the third-order and first-order signal in the reflected signal from the PBG structure. First of all, we have known that the topological charges of third-order and first-order signals are $m_{RF} = m_1 = +1$ and $m_{R1} = m_1 = +1$ according to Eq. (7). Secondly, the nonlinear phase of the first-order and third-order signals in reflected signal induced by field E_2 are $\varphi_{R1} = 2\mathbf{k}_1 n_2^{XE_2} I_2 e^{-\xi^2} z/(n_1 I_{R1})$ and $\varphi_{RF} = 2\mathbf{k}_1 n_2^{XE_2} I_2 e^{-\xi^2} z/(n_1 I_{RF})$, respectively. Furthermore, the first-order signal is more seriously affected by Kerr nonlinearity of field E_2 than the third-order signal because the third-order signal intensity is dominant in the reflected signal as we discussed in the theoretical section. In Fig. 4(a1) and 4(a5), the topological charge of reflected signal is one because the first-order signal and third-order signal in reflected signal are coaxial beams carrying singularities due to the smaller φ_{R1} and φ_{RF} when detuning Δ_2 is far away resonance point $\Delta_2 = -\Delta_1 = -80$ MHz (according to Fig. 1(d)). On the contrary, the first-order signal and third-order signal are non-coaxial beams due to the repulsion along y-direction caused by the Kerr nonlinearity of field E_2 at the resonance point as shown in Fig. 4(a3). The superposition of first-order and third-order beams creates a new leftward fork-like pattern (topological charge -1) between their singularities. Figure 4(b1–b5) are the experimental interferograms of reflected signal carrying phase singularities from PBG structure by scanning the detuning Δ_2. We can see that they are in good agreement with the theoretical results in Fig. 4(a).

4. Conclusions

In conclusion, our analysis of the nonlinear FWM process with different incident angles of the probe has provided a new model of nonlinear spatial filter. We have researched the effect of Kerr nonlinearity to the characters of vortex PTS and FWM images in order to control the new type nonlinear filter. More importantly, we have studied in detail the superposition of first-order and third-order beams in the reflected signal from the PBG structure under the Kerr nonlinearity of dressing field E_2, creating an inverted fork-like pattern in the interferogram.

References

[1] W. Zhang *et al.*, "Experimental realization of entanglement in multiple degrees of freedom between two quantum memories," *Nature Commun.*, vol. 7, 2016, Art. no. 13514.
[2] D.-S. Ding *et al.*, "High-dimensional entanglement between distant atomic-ensemble memories," *Light: Sci. Appl.*, vol. 5, p. e16157, 2016.
[3] L. Allen, M. W. Beijersbergen, R. J. C. Spreeuw, and J. P. Woerdman, "Orbital angular momentum of light and the transformation of Laguerre-Gaussian laser modes," *Phys. Rev. A*, vol. 45, no. 11, p. 8185, 1992.
[4] J. Wang *et al.*, "Terabit free-space data transmission employing orbital angular momentum multiplexing," *Nature Photon.*, vol. 6, pp. 488–496, 2012.
[5] M. F. Andersen *et al.*, "Quantized rotation of atoms from photons with orbital angular momentum," *Phy. Rev. Lett.*, vol. 97, 2006, Art. no. 170406.
[6] G. Molina-Terriza, J. P. Torres, and L. Torner, "Twisted photons," *Nature Phys.*, vol. 3, pp. 305–310, 2007.
[7] M. S. Soskin, V. N. Gorshkov, and M. V. Vasnetsov, "Topological charge and angular momentum of light beams carrying optical vortices," *Phys. Rev. A*, vol. 56, p. 4064, 1997.
[8] G. Molina-Terriza, J. Recolons, and L. Torner, "The curious arithmetic of optical vortices," *Opt. Lett.*, vol. 25, no. 16, pp. 1135–1137, 2000.
[9] H. Wang, D. J. Goorskey, and M. Xiao, "Enhanced Kerr nonlinearity via atomic coherence in a three-level atomic system," *Phys. Rev. Lett.*, vol. 87, no. 7, 2001, Art. no. 073601.
[10] D. V. Petrov, G. Molina-Terriza, and L. Torner, "Vortex evolution in parametric wave mixing," *Opt. Commun.*, vol. 162, no. 4–6, pp. 357–366, 1999.
[11] A. Mair, A. Vaziri, G. Weihs, and A. Zeilinger, "Entanglement of the orbital angular momentum states of photons," *Nature*, vol. 412, pp. 313–316, 2001.
[12] D. P. Caetano *et al.*, "Conservation of orbital angular momentum in stimulated down-conversion," *Phys. Rev. A*, vol. 66, p. 041801, 2002.
[13] G. Walker, A. S. Arnold, and S. Franke-Arnold, "Trans-spectral orbital angular momentum transfer via four-wave mixing in Rb vapor," *Phys. Rev. Lett.*, vol. 108, 2012, Art. no. 243601.
[14] Z. Zhang, D. Ma, Y. Zhang, M. Cao, Z. Xu, and Y. Zhang, "Propagation of optical vortices in a nonlinear atomic medium with a photonic band gap," *Opt. Lett.*, vol. 42, no. 6, pp. 1059–1062, 2017.
[15] Y. Zhang, U. Khadka, B. Anderson, and M. Xiao, "Temporal and spatial interference between four-wave mixing and six-wave mixing channels," *Phys. Rev. Lett.*, vol. 102, no. 1, p. 013601, 2009.

[16] Q.-F. Chen, B.-S. Shi, Y.-S. Zhang, and G.-C. Guo, "Entanglement of the orbital angular momentum states of the photon pairs generated in a hot atomic ensemble," *Phys. Rev. A*, vol. 78, p. 053810, 2008.
[17] M. Cao *et al*., "Demonstration of CNOT gate with Laguerre Gaussian beams via four-wave mixing in atom vapor," *Opt. Express*, vol. 22, no. 17, pp. 20177–20184, 2014.
[18] W. M. Lee, X.-C. Yuan, and W. C. Cheong, "Optical vortex beam shaping by use of highly efficient irregular spiral phase plates for optical micromanipulation," *Opt. Lett.*, vol. 29, no. 15, pp. 1796–1798, 2004.
[19] J. E. Curtis, B. A. Koss, and D. G. Grier, "Dynamic holographic optical tweezers," *Opt. Commun.*, vol. 207, no. 1–6, pp. 169–175, 2002.
[20] A. M. Yao and M. J. Padgett, "Orbital angular momentum: Origins, behavior and applications," *Adv. Opt. Photon.*, vol. 3, no. 2, pp. 161–204, 2011.
[21] D.-W. Wang, H.-T. Zhou, M.-J. Guo, J.-X. Zhang, J. Evers, and S.-Y. Zhu, "Optical diode made from a moving photonic crystal," *Phys. Rev. Lett.*, vol. 110, 2013, Art. no. 093901.
[22] Z. Wang, M. Gao, A. R. Mahesar, and Y. Zhang, "Phase modulation of photonic band gap signal," *Sci. Rep.*, vol. 6, 2016, Art. no. 28185.
[23] Y. Zhang *et al*., "Four-wave mixing dipole soliton in laser-induced atomic gratings," *Phys. Rev. Lett.*, vol. 106, no. 9, 2011, Art. no. 093904.